JOURNAL OF MATERIALS SCIENCE 25 (1990) 1184–1196

Magnesium rheocasting: a study of processing–microstructure interactions

ANTOINE TISSIER, DIRAN APELIAN
Materials Engineering, College of Engineering, Drexel University, Philadelphia, Pennsylvania 19104, USA

GILLES REGAZZONI
Pechiney Research Centre, BP 27, 38340 Voreppe, France

The rheocasting solidification process has been applied in the production of AZ91D magnesium alloy. A batch-type rheocaster has been designed to produce rheocast ingots in an argon-covered, closed chamber system, under different processing conditions. Processing variables which were evaluated include shear rate, isothermal stirring time and volume fraction solid during isothermal stirring. A detailed examination was made of the resultant microstructure using three different techniques to reveal the rheocast structure: etching techniques, reheating at the isothermal stirring temperature and quenching, and scanning microscopy via backscattering techniques. Rheocasting yielded a non-dendritic structure, wherein the primary phase has a rosette-shaped morphology surrounded by a divorced eutectic. The evolution of the structure and the morphological changes which occur during processing are described. The uniformity in the primary particle size, as well as their sphericity, was increased by increasing the stirring time, or the shear rate, or by decreasing the stirring temperature (increasing the volume fraction solid present). Increasing the shear rate gave rise to a more efficient break-up of the dendritic structure. Porosity was present in the samples which was detrimental to the mechanical properties; however, the mechanical properties after extrusion were quite outstanding.

1. Introduction

For over a century and until the 1940s, magnesium metal was a scientific curiosity. In the early 1800s magnesium was first discovered by Sir Humphrey Davy, who in 1808 reported the production of magnesium in the form of an amalgam, and later on in 1828 Bussy first produced magnesium in metallic form. From the 1830s until the 1940s, the use of magnesium as an engineering material was in a dormant state. The outbreak of World War II brought on a resurgence and a need for the utility of magnesium and its alloys. Since then, magnesium alloys have become to be recognized as useful engineering materials.

Magnesium is a light material; it has a density of 1.74 with excellent mechanical strength. In comparison with aluminium, it is 35% lighter and the material cost on the basis of volume is more favourable. It possesses excellent castability and machinability, and its high thermal conductivity allows rapid-cycle casting which is one of the major reasons for its wide use as a die-casting material. The main limitation of magnesium metal has been its reactivity and corrosion. However, over the last decade significant improvements have been made in this area by compositional control of the alloy–for example, by lowering impurity elements such as the transitional elements.

Rheocasing and thixocasting are processes which have been developed during the early 1970s. During the last decade rheocasting of aluminium, copper and superalloys has resulted in the production of components having minimum segregation. Dow Chemical has recently investigated the feasibility of slurry-casting magnesium using an injection moulding technology [1, 2]. The objective of this work was to study the rheocasting process as it is applied to magnesium alloys and to characterize the effect of process variables on the rheocast microstructure.

2. Rheocasting: the process

2.1. Rheocasting

Rheocasting is the production and casting of semi-solid slurries. It involves the melt being cooled into the mushy zone with the mechanical stirring started while the alloy is fully liquid. Subsequently, the melt can be isothermally held at a given temperature (Fig. 1), corresponding to a certain fraction solid, while stirring continues. Rheocast metal has been produced at volume fractions of solid ranging up to about 70% [3]. Rheocast slurries show a hysteresis loop phenomenon similar to other well-known thixotropic systems [4]. Various alloys have been rheocast either in a batch or a continuous mode, and work has been reported on aluminium-base [5–7], copper-base [8], Pb–Sn [9], iron-base [10], cobalt-base [11] and nickel-base [12] alloys. Fig. 2 is a schematic diagram of a continuous rheocasting machine proposed by Flemings [3]. The basic rheocasting concept has

0022-2461/90 $03.00 + .12

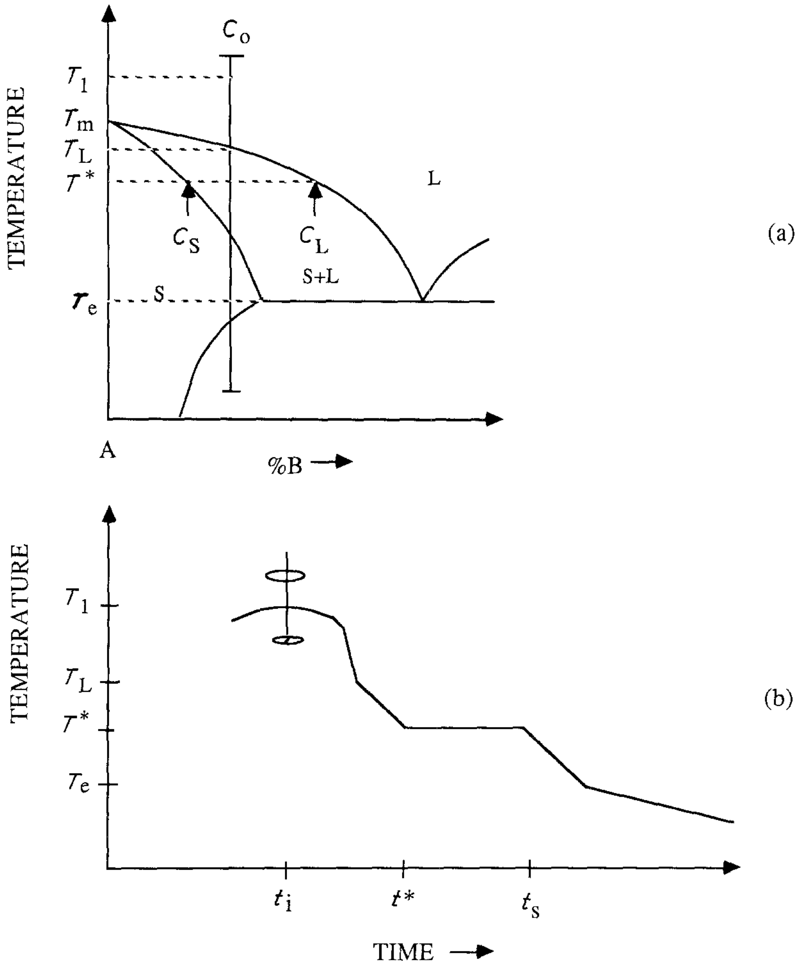

Figure 1 (a) A portion of the phase diagram for the generic system A–B showing the two-phase region; alloy of composition C_0 is processed by lowering its temperature along the isoconcentration line at C_0. (b) A generic diagram of the rheocasting process described by a temperature–time plot. Stirring is initiated at time t_i while the melt is at a temperature T above T_L. The slurry is isothermally held at temperature T^* for a period $t_s - t^*$). At t_s, the stirring is stopped and the slurry is cast.

been extended to produce composite materials and wrought-slurry castings.

2.2. Rheocast structure

Previous work on rheocasting has shown that the resultant microstructure is controlled by four independent processing variables: volume fraction of primary solid particles (stirring temperature), shear rate, stirring time and cooling rate [3–18]. The following processing effects have been reported [19]:

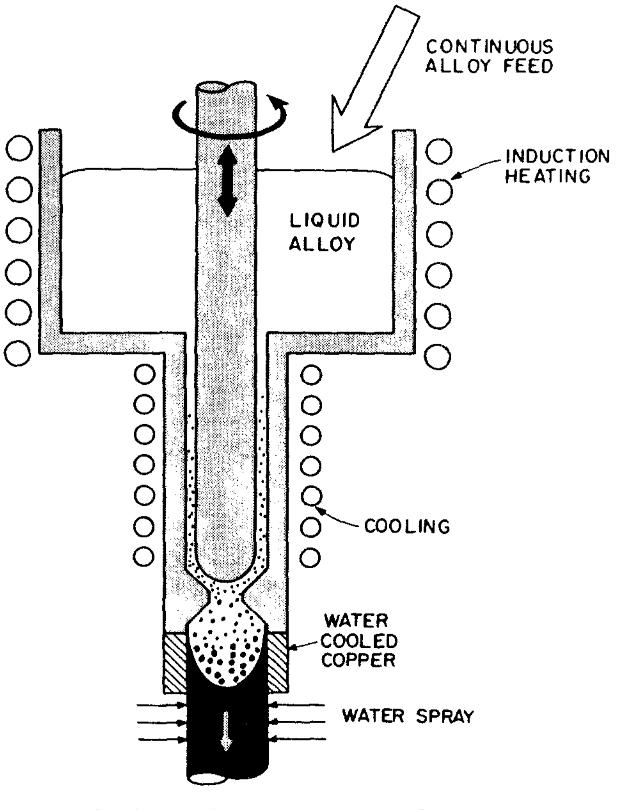

Figure 2 Continuous rheocaster apparatus [3].

(i) The primary solid particle size decreases as shear rate increases. In addition, as the volume fraction solid increases, larger primary solid particles are observed.

(ii) Increasing shear rate, stirring time or volume fraction solid increases the sphericity of primary solid particles; this corresponds to fragmentation of the dendrite arms to give individual grains that are more spherical in shape. However, this fragmentation is often only partial, resulting in modified segments of dendrites which are described as rosette-like cells. Fig. 3 shows the effect of shear rate on the resultant viscosity of the slurry.

Rheocast structures offer the following advantages over conventional cast structures [3–20]:

(i) reduced shrinkage pipe and the potential for crack formation,

(ii) uniformly distributed microporosity (if present),

(iii) formation of a fine and non-dendritic grain structure, and

(iv) reduced micro- and macro-segregation.

2.3. Mechanism of rheocasting

This topic has been reviewed by Doherty *et al.* [17] in terms of a grain boundary model initially proposed by Vogel *et al.* [21]. In order to explain both the initial fragmentation of a dendritic structure by stirring [19] and the build-up and break-down of agglomerated solid particles [4], the formation of grain boundaries and their dissolution by liquid wetting has been postulated. The initial formation of grain boundaries in single-crystal dendrites was suggested as occurring by plastic bending of secondary dendrite arms, folowed by recrystallization to give grain boundaries whose total misorientation would be that of the angle through which each arm has been bent. Fragmentation of the now polycrystalline dendrite could then occur either by liquid phase wetting, or possibly by grain boundary sliding. Agglomeration of groups of particles could occur by a sintering mechanism where grain boundaries form. Such clustering is known to occur when the stirring rate is reduced [4, 17].

In conclusion, this model predicts two types of grain boundary. One is formed by solid-state recrystallization where the solute content of the region close to the new grain boundary is unchanged by the process; the other type of boundary is formed by the sintering of solid particles and should show solute enrichment arising from the typical pattern of microsegregation. Both types of boundary have been found in various low melting point alloys [17].

3. Experimental procedure

3.1. Scope of experiments

The scope of experiments involved the following:

(i) design and build a rheocasting apparatus for magnesium;

(ii) characterize the evolution of the rheocast structure vis à vis conventionally cast material;

(iii) investigate the effect of the significant rheocasting process variables on the resultant structure; and

(iv) evaluate the mechanical properties of a magnesium alloy cast by different routes and subsequently extruded.

3.2. Materials

The magnesium alloy selected for this study was the AZ91D alloy. The nominal composition of the alloy is given in Table I. The alloy has a wide melting range, as can be seen in the phase diagram given in Fig. 4. This is beneficial in the rheocasting process since it allows the operator greater flexibility.

The following differently processed AZ91D samples were evaluated:

(i) die-cast alloy (as-received material),

(ii) as-received material which was remelted in a permanent steel mould (as-cast material),

(iii) rheocast material solidified in a permanent steel mould, cast under different imposed cooling rates (from water-cooling to air-cooling),

(iv) rheocast and as-cast materials which were subsequently extruded.

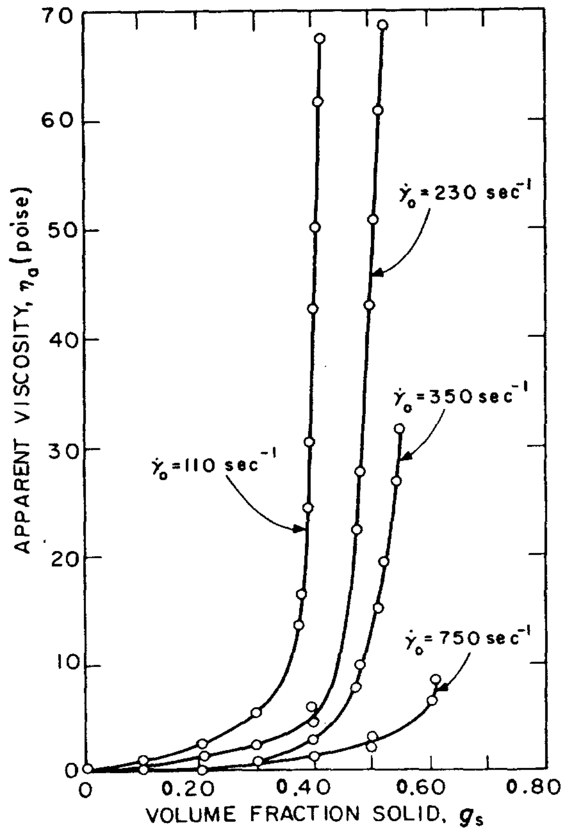

Figure 3 Viscosity of Sn–15% Pb alloy against fraction solid for different applied shear rates during processing [3]. Sn–15% Pb, ε = 0.33°C min^{-1}, continuously cooled. 1 poise = 10^{-1} Pa sec.

3.3. Apparatus

The rheocasting apparatus which was used in this study is shown in Fig. 5. The rheocaster is specially designed for magnesium alloys; the process is carried out in an argon-covered, closed chamber system. The set-up is a batch-type rheocaster: subsequent to stirring, the slurry is allowed to solidify in the steel crucible. The impeller shaft and the impeller itself are machined out of 304 stainless steel.

The alloy charge was melted in the crucible (coated with boron nitride), using a cylindrical electrical furnace surrounding the crucible. The furnace is placed on a mechanical rig allowing it to be lowered and raised. Upon termination of stirring (at time t_s, see Fig. 1b), the furnace is lowered and the chamber may be cooled in a variety of different ways giving rise to different cooling rates: the chamber containing the crucible can be air-cooled (AC), or water-cooled (WC) via water-cooled copper pipes surrounding the chamber, or water-quenched (WQ) by plunging the chamber into a water bath.

Stirring of the melt and the slurry were carried out by the impeller whose shaft is attached to a motor by a pulley belt. The range of rotation speeds was 200 to 610 r.p.m. The speed of the impeller was calibrated by a stroboscope. Temperature of the melt/slurry was

TABLE I Composition of AZ91D alloy (wt %)

Mg	Al	Zn	Mn	Si	Cu	Ni	Fe	Other impurities
bal.	8.5–9.5	0.5–0.9	$\geqslant 0.15$	$\leqslant 0.02$	$\leqslant 0.015$	$\leqslant 0.001$	$\leqslant 0.005$	$\leqslant 0.01$

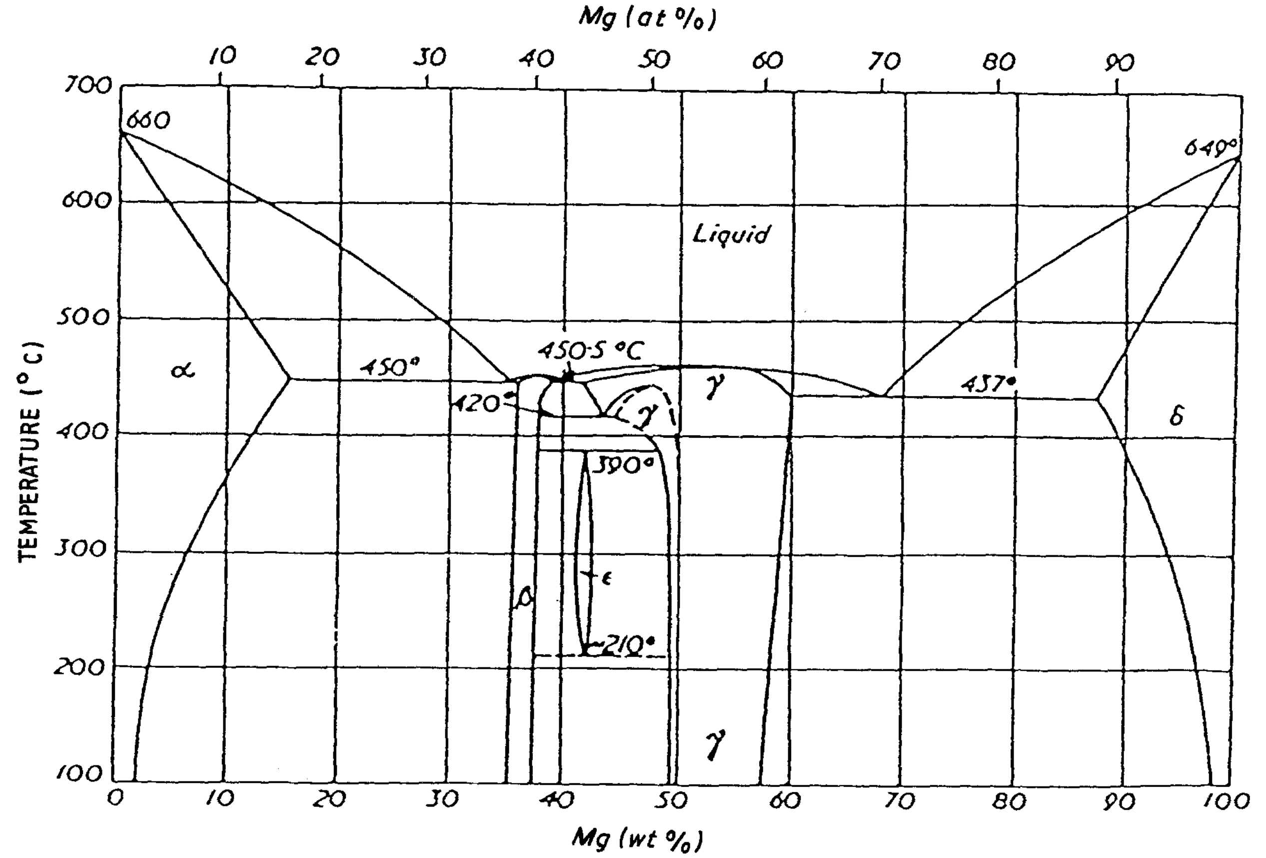

Figure 4 Al–Mg binary phase diagram.

monitored using a K-type thermocouple placed in the melt near the inner wall of the crucible.

3.4. Processing

As can be noted in Fig. 1, the isothermal hold at T^* is an important variable since it affects the fraction solid present in the slurry. Thus a prerequisite was to determine the calibration curve relating temperature with the fraction solid present in the slurry. Fig. 6 shows temperature as a function of the fraction solid: this was obtained by applying the lever rule to the equilibrium Mg–Al binary phase diagram. It is interesting to note that over a temperature range of 30° C the fraction solid varies from 0 to 0.45.

The starting material-charge ranged from 1 to 1.4 kg. The charge is placed in the steel crucible and heated to T_l (above the liquidus) at time t (see Fig. 1). The rotating impeller is lowered into the melt; the speed of rotation is controlled by a rheostat. Whilst being stirred the temperature of the melt is lowered to T^* where is is isothermally held for a given period of time ($t_s - t^*$) ranging from 15 to 120 min. Subsequently, the impeller is removed, the furnace is lowered, and the slurry is allowed to solidify.

Over 25 different rheocasting runs were carried out. Some were scoping experiments and others were tests for reproducibility. Table II lists the processing variables used for each run.

TABLE II Rheocasting experiments

Run No.	Charge mass (kg)	T^* (° C)	f_s[†]	Stirring rate (r.p.m.)	($t_s - t^*$)[‡] (sec)	Cooling mode[§]
I	1.2	567 +2/−1	0.45	200	900	AC
II	1.05	572 +1/−1	0.40	200	900	AC
III	1.2	577 +0/−1	0.32	200	900	AC
IV	1.1	582 +2/−3	0.24	200	900	AC
V	1.3	577 +2/−3	0.32	200	2700	AC
VI	1.3	577 +1/−3	0.32	400	900	AC
VII	1.3	572 +2/−2	0.40	500	900	AC
VIII	1.4	572 +2/−2	0.40	200	900	WC
IX	1.5	576 +2/−1	0.33	610	900	WQ
X	1.5	576 +1/−1	0.33	610	7200	WC
XI	1.5	576 +1/−1	0.33	610	7200	WC
XII	1.5	576 +1/−1	0.33	610	7200	WC
XIII	2.3	576 +2/−2	0.33	0	3600	AC

[†] f_s is the fraction solid at temperature T^* (Fig. 1).

[‡] Isothermal hold time at T^* (Fig. 1) while the slurry is stirred.

[§] Cooling mode applied to the crucible at time t_s (Fig. 1) after isothermal hold: AC = air cooled, WC = water-cooling of chamber. WQ = water-quenching of chamber by plunging it in a water bath.

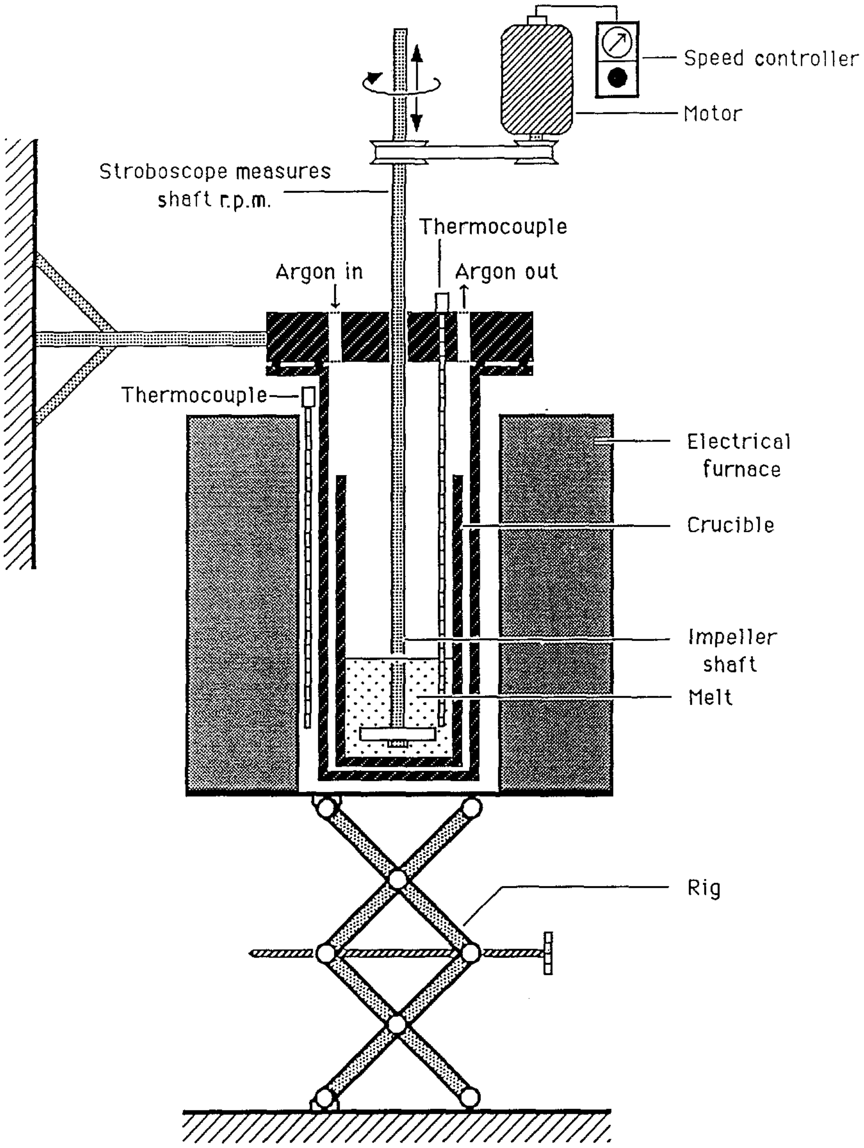

Figure 5 Schematic diagram of a batch-type rheocaster used for processing magnesium alloys.

Runs I to IV (Table II) were designed to investigate the effect of T^* on the resultant rheocast microstructure; run V served the purpose of observing the effect of a prolonged isothermal hold time, whereas runs VI and VII were carried out to study the influence of stirring speed or shearing rate. Subsequent to stirring, the impeller was removed and the chamber was air-cooled. For runs VIII and IX the chamber was water-cooled and water-quenched, respectively. The apparatus was pushed to its limit in terms of stirring speed – 610 r.p.m. – for Run X. Runs XI and XII were processed similarly to Run X; however, here the rheocast ingots were extruded. Extrusion conditions were as follows: diameter ratio 20, speed of the piston $0.5\,\mathrm{sec}^{-1}$, temperature 250° C, pressure 165 bar (1.65×10^7 Pa).

For comparison, the as-received material (die-cast) was remelted in the rheocasting apparatus without any mechanical stirring (Run XIII).

3.5. Reheating experiments

To distinguish and to delineate the primary solid phase from the liquid phase during rheocasting at the point of impeller removal, the following experimental technique was used: it consisted of reheating the sample to T^* – the temperature at which it was isothermally held – and rapidly quenching the sample. In the reheating experiments the specimens were isolated and protected in aluminium ampoules while quenching them in a water bath.

3.6. Microstructure characterization

The microstructure of rheocast specimens were examined

(i) to determine the level of porosity in the rheocastings produced,

(ii) to identify the phases observed, and

(iii) to describe the evolution and solidification of the rheocast structure.

Samples were cut and polished using diamond paste down to $1\,\mu$m; subsequently, solution of 0.5 and $0.03\,\mu$m magnesia were used. Two different etchants have been used: phospho-picral etchant containing 0.7 ml H_3PO_4, 5 g picric acid, and 100 ml ethanol (95%), and a solution of $60\,\mathrm{cm}^3$ ethylene glycol, $20\,\mathrm{cm}^3$ acetic acid, $20\,\mathrm{cm}^3$ of water and $1\,\mathrm{cm}^3$ nitric acid. A Tracor image analyser was used to quantify the level of porosity in the rheocast samples. A Zeiss ICM 405 microscope was used to study the rheocast microstructure, and a Tracor SEM-EDS was used to identify the phases observed by scanning electron

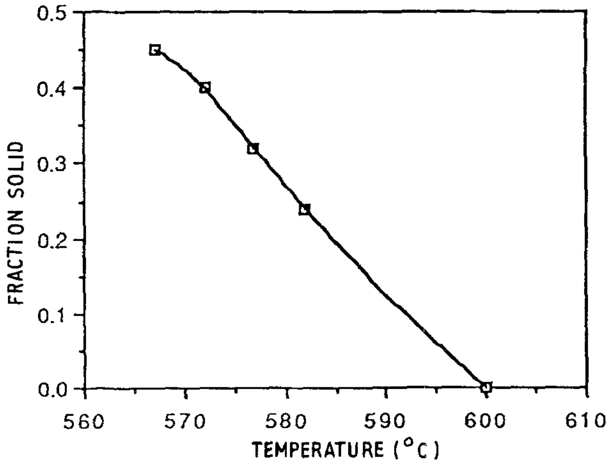

Figure 6 Variation of fraction solid as a function of temperature (specifically the isothermal hold temperature T^*) for the AZ91D magnesium system.

microscopy (SEM) and energy dispersive spectroscopy (EDS).

3.7. Mechanical properties

Specimens from the processed materials, shown in Table II, were evaluated for mechanical properties. Both micro- and macro-hardness tests were carried out using a LIM Vickers hardness apparatus. A load of 10 kg was used in the macrohardness tests. Tensile properties at room temperature were also evaluated for the processed materials shown in Table II. ASTM E8 specifications and standards were followed.

4. Results

The results of the rheocasting experiments and the effects of the processing variables on the resultant rheocast structure are presented. In addition, mechanical property results of cast and extruded material are given.

4.1. The rheocast structure

The macrostructure of the rheocast product in comparison with the structure obtained through other processing means is shown in Fig. 7. Figs 7a and b are micrographs of die-cast magnesium AZ91D alloy at different magnifications. The dendritic structure can be noted in Fig. 7a; the structure is very fine with an average dendrite arm spacing (DAS) of 40 μm. The eutectic phase, as a result of the last liquid to freeze, is found within the interdendritic regions. The alloy cast in the same crucible, and under similar conditions as the rheocast material, but without any imposed stirring (as-cast material), presents a much coarser structure than the diecast alloy (Figs 7c and d). The average DAS spacing of the as-cast sample is 74 μm. Upon freezing, the intercellular liquid precipitates out the α and the $MG_{17}Al_{12}$ phases as the liquid approaches the ternary eutectic composition. In Fig. 7d, the $Mg_{17}Al_{12}$ massive phase can clearly be seen. This is surrounded by the lamellar structure of α and $Mg_{17}Al_{12}$; such a divorced form of the eutectic is a classical feature of the AZ91D alloy [22].

The microstructure seen in Figs 7e and f is typical of rheocast structures [3]: the lack of a distinct dendritic network is noticeable. The dendritic islands have been broken up to form spherical and rosette-like cells, having a typical size of a few hundred micrometres. As in the previously discussed microstructures, the rounded cells are surrounded by the last liquid to freeze; the divorced eutectic can be seen surrounding the cells (Fig. 7f).

Porosity is caused by shrinkage, gas entrapment and insufficient liquid to fill intercellular/interdendritic regions. Moreover, in the rheocast ingots, porosity might have been induced by the removal of the impeller. Porosity of the die-cast samples was very low, ~0.002%, confirming that the die-cast material possessed excellent metallurgical integrity. Porosity in the as-cast material was higher than the die-cast material, ~0.05%.

In the rheocast ingots, the observed pores were heterogeneously distributed. For example in Run III, the level of porosity at the top of the ingot was measured to be 0.13%, at the centre 1.6%, and at the bottom 0.22%.

To study and compare processing effects on the resultant porosity in the rheocast ingots, porosity at the centre of the ingot was measured. Porosity varied from 0.08 to 5.21%, and no significant dependence of the level of porosity on the rheocast processing conditions was observed (Fig. 8). There is only a trend that porosity is lower for rheocast ingots which were processed at a low fraction solid (higher T^* in Fig. 1). When the stirring is carried out at a high isothermal temperature, there is more liquid present and feeding occurs more readily than in the case in which the melt is processed at a high fraction solid in the slurry. The scatter of these results is probably due to the extra porosity induced during the removal of the impeller.

SEM analysis was used to identify some microstructural features observed in the rheocast samples. Fig. 9 is a backscattered electron image of a representative rheocast structure. The composition of the rosette like cell is 94.9 wt% Mg, 4.5 wt% Al, 0.5 wt% Zn, 0.1 wt% Mn. It is interesting to note that for the sample examined, the stirring temperature was 576° C (Table II), which corresponds to an equilibrium aluminium composition of 4.5%, the same value of the aluminium content as in the rosette-like cell. The envelope surrounding the cells is the last liquid to freeze, and is rich in solute aluminium. During the solidification process the precipitation of the $Mg_{17}Al_{12}$ phase occurs as can be seen in Fig. 9a; the actual composition of this phase is 54.6 wt% Mg, 41.2 wt% Al, 4.2 wt% Zn. It is important to note that the $Mg_{17}Al_{12}$ phase (the aluminium-rich phase, shown in bright contrast on the scanning micrograph of Fig. 9a) is one of the reaction products formed during freezing of the intercellular liquid. The lamellar phase being magnesium-rich (90% magnesium) cannot be revealed by the backscattered electron image. Within the intercellular liquid as well as in the cells, small precipitates are noted, and these precipitates were found to be extremely low in magnesium content and rich in manganese. The composition of the precipitates is 45.2% Al, 53.5 wt% Mn, 1.3 wt% Mg. These manganese–aluminium intermetallics are present in

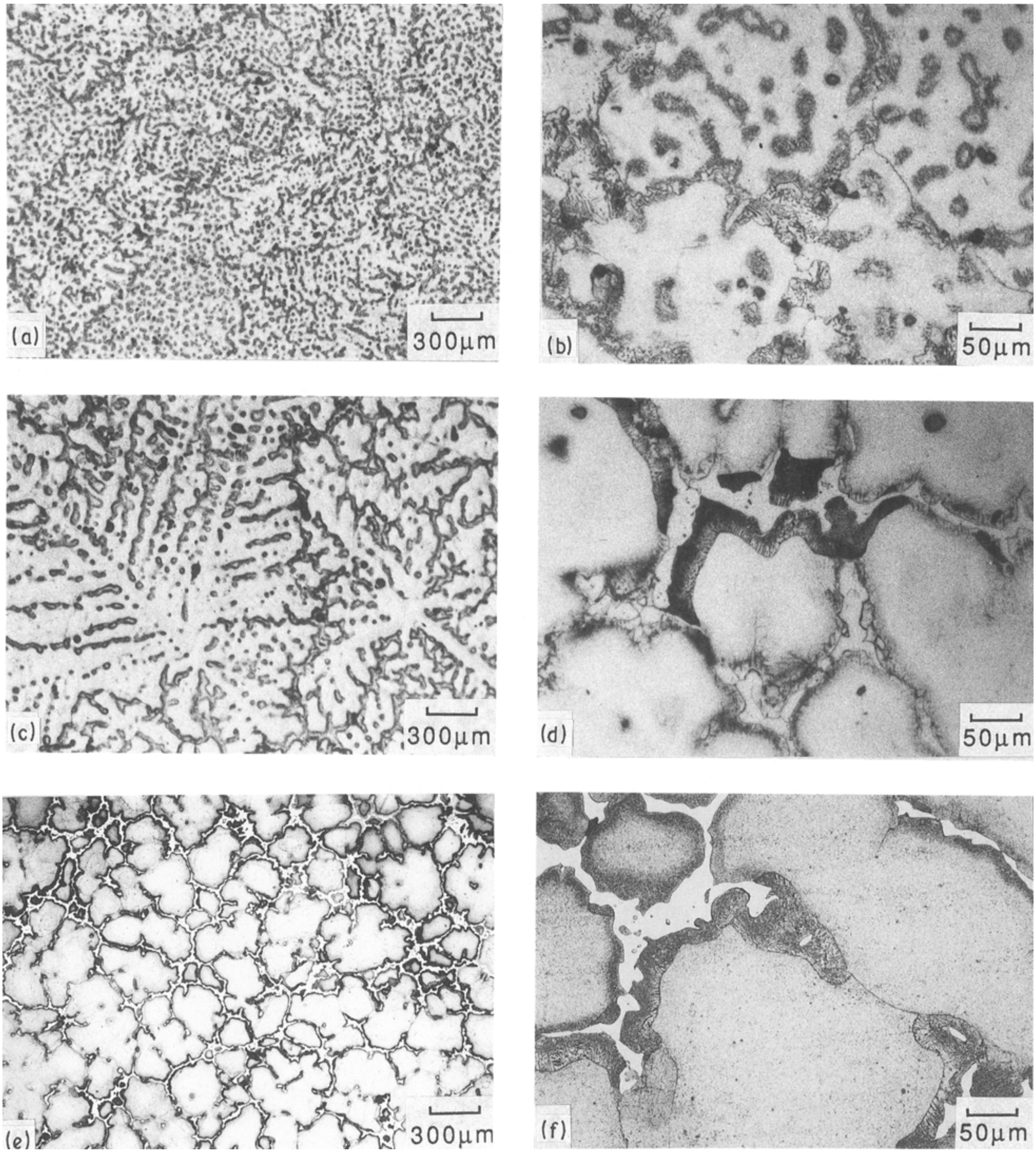

Figure 7 Photomicrographs revealing the microstructure of differently processed magnesium alloy AZ91D: (a, b) die-cast material, (c, d) as-cast material, (e, f) rheocast material.

the die-cast material, the as-received material. The melting point of these intermetallics is much higher than the melting point of magnesium, and during rheocasting the manganese-rich intermetallics are not fully remelted. Another precipitate, which has a distinctly different morphology, was observed in some of the rheocast samples. These precipitates are needle-like and have been identified as Al_3MgMn.

Within a single cell, different contrasts can be observed as shown in zones A, B and C of Fig. 9. The origins of these contrasts were further studied by SEM–EDS analysis which provided composition profiles across the cell. It can be noted in Figs 9b and c that the magnesium content across the length of a cell (rosette) did not vary, and was measured to be constant close to 95 wt %, which is the value of the equilibrium magnesium content at the agitation temperature. The rheocasting experiments were carried out at relatively high temperatures in the mush zone, and the slurry was stirred isothermally (T^*) for relatively long periods. Furthermore, cooling was rather slow. These conditions promote diffusion and homogenization within the cell.

It is interesting to note the variation of aluminium content within a given cell. Along profile AC the aluminium content varied, suggesting that the cell which is being addressed comprises two sub-cells which have sintered together. On the other hand, the aluminium content was constant along profile AB. The contrasts observed within the cell are

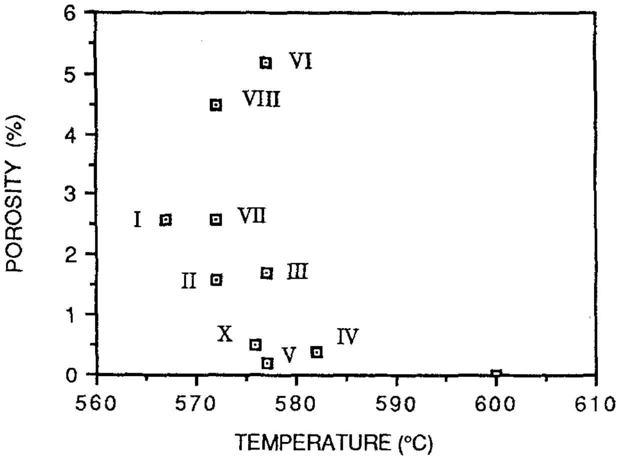

Figure 8 Porosity against rheocasting temperature T^*.

crystallographic contrasts developed during the formation of the cell. First, subgrain boundaries are developed due to bending of the dendrite arm during agitation, resulting in two subgrains having different orientations without aluminium-rich liquid infiltrating between them. A good example is given in Fig. 9c by zones A and B. Doherty and Vogel's theory [17, 21] for dendrite arm bending predicts such a structure (non-wetting case).

Secondly, the sintering of primary islands or subcells is expected; it has been shown that during isothermal hold, smaller primary islands coalesce and sinter together due to the imposed stirring or during cooling [17]. This is illustrated in Fig. 9b by zones A and C; however, is is not possible to discern from these structures whether coalescence occurred during the isothermal hold time or subsequently during cooling.

Fig. 10 shows a given selected area in the rheocast structure; the same area is shown after polishing (Fig. 10a), etching for a few seconds (Fig. 10b), and after polishing but observed under interference contrast (Fig. 10c). In Fig. 10a, the cells surrounded by the $Mg_{17}Al_{12}$ phase are seen. However, when etched, the primary solid cells present during the isothermal hold time are revealed as can be seen by the dark envelopes (etching effect) around each primary solid island (Fig. 10b). Moreover, the delineation of the α and $Mg_{17}Al_{12}$ phases can be seen. The former is immediately adjacent to each primary cell, whereas the $Mg_{17}Al_{12}$ phase is found in the interconnecting spaces. Fig. 10c is a relief map of the same area showing this composite structure.

To support these observations, reheating experiments were carried out to analyse the rheocast microstructure. Samples were cut from the rheocast ingots and were reheated to the isothermal hold temperature, T^*, stabilized at this temperature and then quenched. This procedure imposes a high cooling rate during solidification of the intercellular liquid, thus allowing one to delineate the primary islands from the intercellular liquid. Figs 11a and b allow a comparison of the structures of two specimens from Run III: as rheocast (Fig. 11a) and after reheating and quenching (Fig. 11b). Figure 11b clearly delineates the primary islands from the surrounding aluminium-rich liquid. One can also notice that Figs 11a and b are very similar, giving validity to this technique of analysis.

4.2. Effect of processing variables on the rheocast structure

The effect of stirring time during rheocasting is shown in Figs 11a (Run III) and 11c (Run V). Fig. 11a reveals a bimodal distribution of particle size $\approx 20\,\mu m$ and another greater than $100\,\mu m$. However, when the stirring time is increased, this bimodal distribution changes character: the larger dendritic-like particles become rounded, and the smaller ones coalesce and gather forming clusters.

The effect of the isothermal hold temperature prior to terminating agitation and solidifying the slurry can be seen by the micrographs shown in Figss 11a

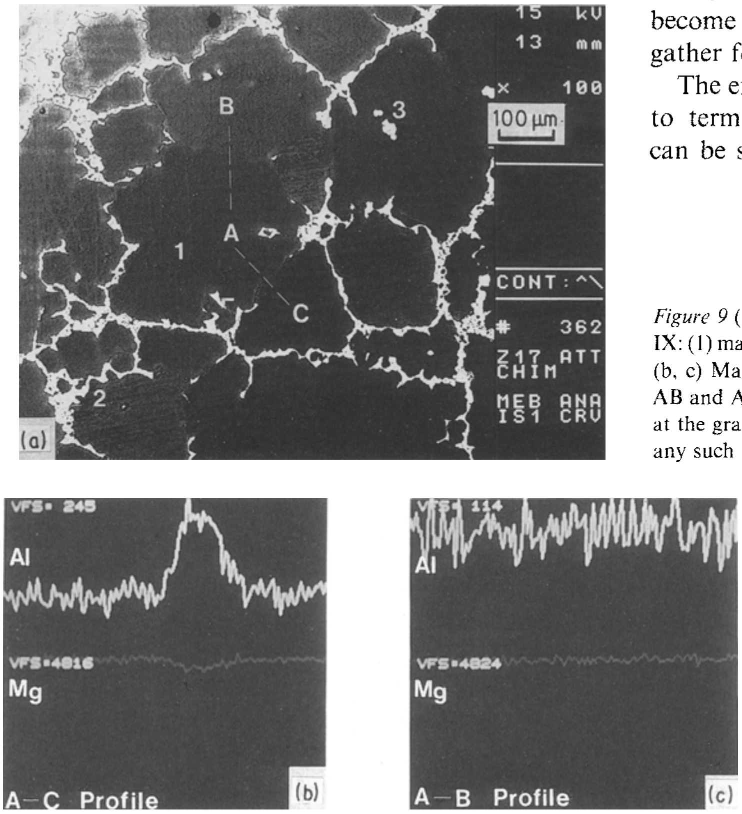

Figure 9 (a) SEM backscattered electron image of rheocast sample IX: (1) magnesium-rich matrix, (2) $Mg_{17}Al_{12}$phase, (3) AlMn phase. (b, c) Magnesium and aluminium content profiles along the lines AB and AC. In (b) the EDS profile reveals aluminium enrichment at the grain boundary while in (c) the EDS profile does not reveal any such enrichment.

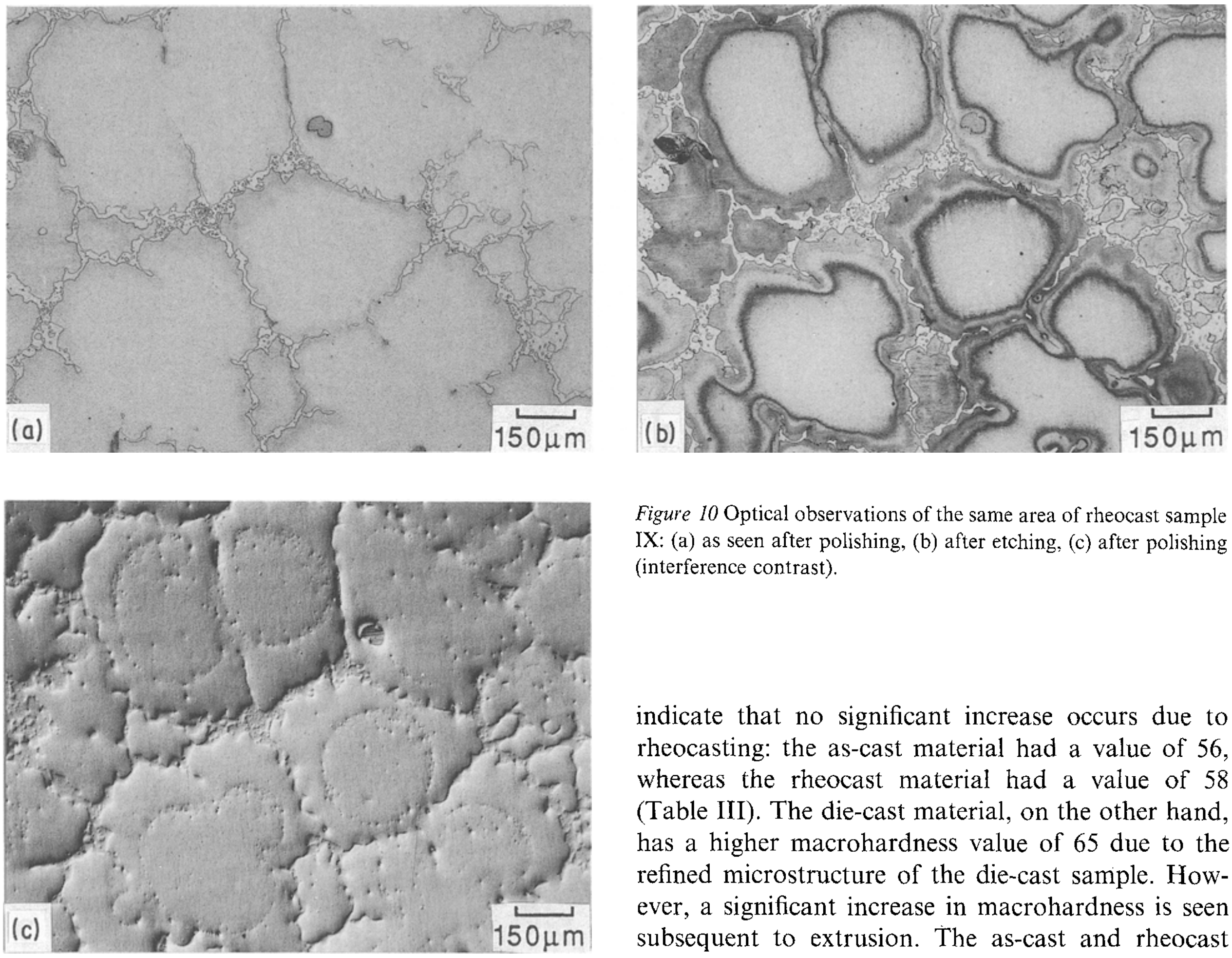

Figure 10 Optical observations of the same area of rheocast sample IX: (a) as seen after polishing, (b) after etching, (c) after polishing (interference contrast).

and d. As the volume fraction solid is increased, the sphericity of the primary island or cells is increased. This is due to a higher effective shear rate when there is a larger volume fraction solid in the slurry, even though the stirring speed is kept constant (see Fig. 3). In addition, at a higher volume fraction solid a bimodal distribution of particle size is not observed.

The effect of shear rate during processing is clearly seen by the microstructures from Runs II and VII (Figs 12a and b). In the former, the stirring speed was 200 r.p.m. and in the latter 500 r.p.m. In both cases, the fraction solid present and the stirring time were kept fixed at 577° C and 15 min. It is observed that the higher shearing rate (Fig. 12b) gives rise to a more efficient break-up of the dendritic structure, resulting in smaller primary cells. It can also be noticed that the primary cells appear to be rounder when the stirring speed is higher.

The rheocast structures from samples which were air-cooled, water-cooled, or water-quenched subsequent to isothermal hold did not show significant differences. This can be attributed to the volume of materials which needed to be quenched and to apparatus limitations.

5. Mechanical properties

Microhardness test results indicated that the rheocast cells have an average hardness of 47, whereas the intercellular phase is much harder and has an average value of 132. Macrohardness results (averaged values) indicate that no significant increase occurs due to rheocasting: the as-cast material had a value of 56, whereas the rheocast material had a value of 58 (Table III). The die-cast material, on the other hand, has a higher macrohardness value of 65 due to the refined microstructure of the die-cast sample. However, a significant increase in macrohardness is seen subsequent to extrusion. The as-cast and rheocast extruded samples have average hardness values of 78 and 73, respectively. A 25% increase in hardness is realized upon extrusion.

A similar trend is observed with the results of the tensile tests. The results are shown in Table III. The tensile properties of the rheocast specimens are not very credible due to the high level of porosity in the material. Considerable improvement in the tensile properties is obtained upon extrusion of the as-cast and rheocast samples. After extrusion, the rheocast and the as-cast samples have very similar properties and the results clearly indicate the beneficial effect of thermomechanical processing subsequent to rheocasting. Moreover, the tensile property results of the extruded materials show high strengths with good ductility. Such a combination of strength and ductility is very desirable and points out the potential of the AZ91D alloys as a wrought alloy.

6. Discussion

Rheocasting of the slurry produces a non-dendritic structure, wherein the primary phase has rosette-shaped morphology surrounded by a divorced eutectic. Moreover, macrosegregation throughout the cast structure is reduced in contrast to conventionally cast material. Microstructural features of rheocast components are affected by processing variables such as volume fraction solid present, shearing rate, stirring time, and to some extent the cooling rate imposed subsequent to the isothermal hold period.

The rheocast structures which have been studied are all "frozen-in" structures analysed at room temperature. Fig. 13 is a schematic diagram which

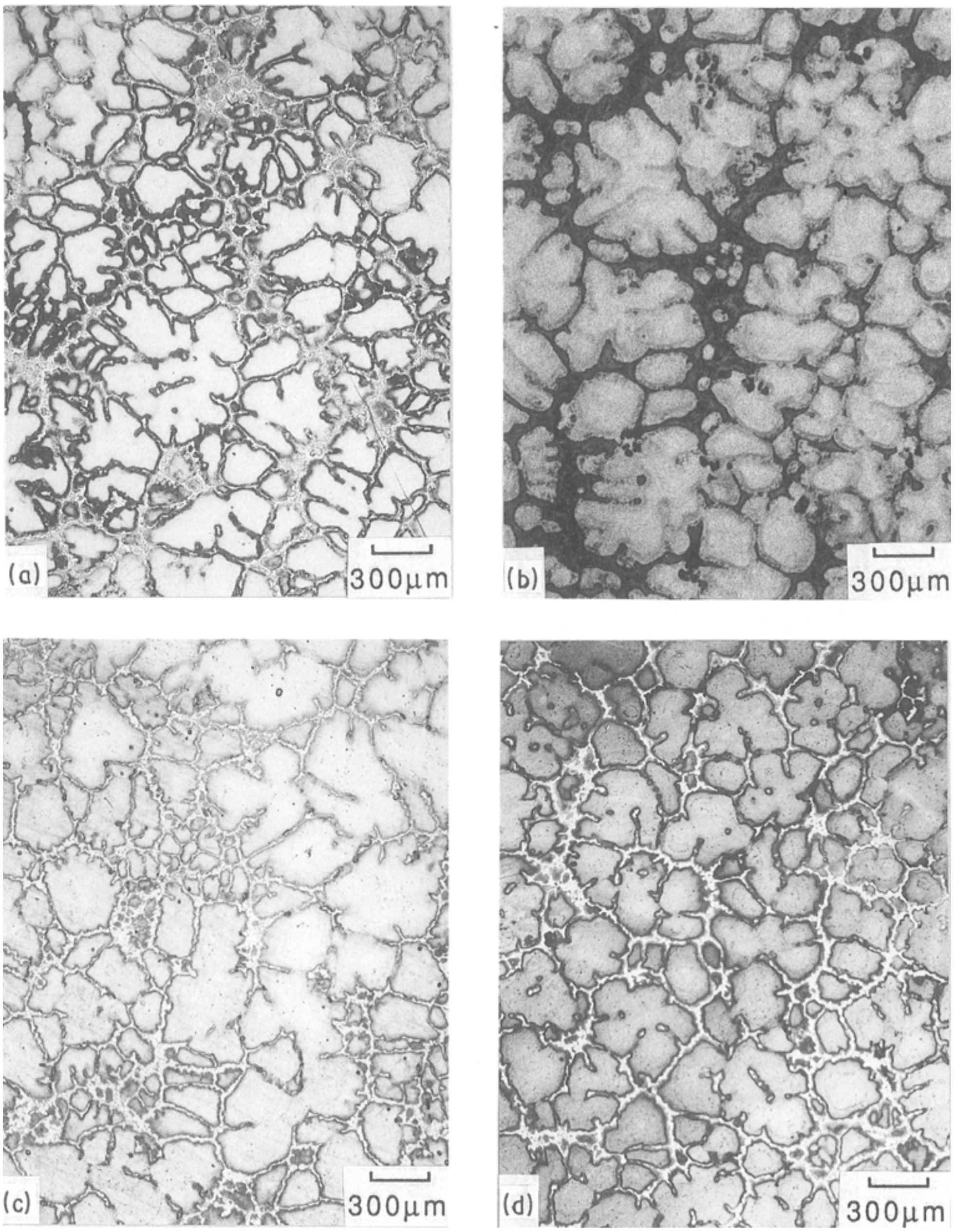

Figure 11 Microstructures after etching of rheocast samples processed in different conditions: (a) run III, $T^* = 577^\circ$C, 200 r.p.m. $t_s = 900$ sec, air-cooled; (b) same sample after reheating at T^* and quenching; (c) run V (showing the effect of a longer stirring time t_s, compared with (a)), $T^* = 577^\circ$C, 200 r.p.m., $t_s = 2700$ sec, air-cooled; (d) run I (showing the effect of a lower rheocast temperature T^* when compared to (a)), $T^* = 562^\circ$C, 200 r.p.m., $t_s = 900$ sec, air-cooled.

TABLE III Hardness and tensile properties of differently processed AZ91D alloy samples

Property	Treatment				
	Die-cast	As-cast*	Rheocast†	As-cast, extruded‡	Rheocast, extruded‡
Hardness ($\mathrm{kg\,mm^{-2}}$)	65	56	58	78	73
Tensile yield stress (MPa)	124	120	(83)	226	215
Tensile strength (MPa)	170	170	(92)	313	296
Total elongation (%)	3	2	0.3	15.6	10.2

*Received die-cast material subsequently remelted in rheocasting crucible without agitation.
†Average results of all rheocast samples evaluated.
‡Extrusion conditions: diameter ratio 20; piston speed 0.5 $\mathrm{mm\,sec^{-1}}$; temperature 250° C; pressure 165 bar (1.65×10^7 Pa).

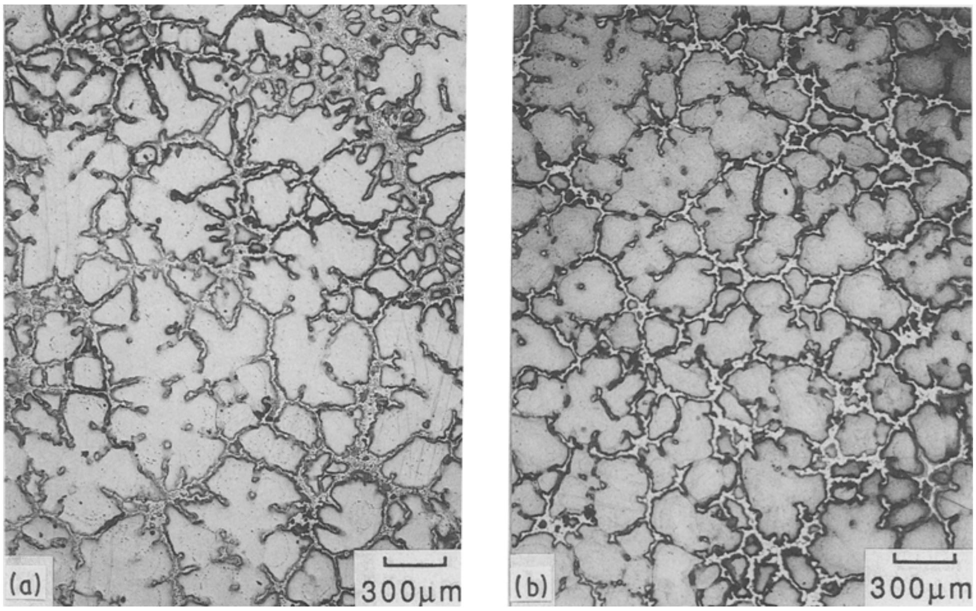

Figure 12 Microstructures after etching of rheocast samples processed at different shearing rates: (a) run II, $T^* = 572°\mathrm{C}$, 200 r.p.m., t_s = 900 sec, air-cooled; (b) run VII, $T^* = 572°\mathrm{C}$, 500 r.p.m., t_s = 900 sec, air-cooled.

describes the evolution of the structure and the morphological changes which occur during processing. The melt is cooled down to the liquidus temperature and dendrites are formed which are simultaneously fragmented due to the imposed agitation. For a fixed stirring speed, a lower isothermal hold temperature or a slurry containing a higher fraction solid results in an increased shear level. The higher the imposed shearing rate, the more vigorous is the phenomenon of dendrite fragmentation.

During agitation of the slurry, some of the dendrite arms are bent causing the formation of subgrains having different orientations. If the aluminium-rich liquid does not wet the subgrain boundary, the subgrains do not split and aluminium-enriched region cannot be observed between the subgrains. On the other hand, if the aluminium-rich liquid wets the subgrain boundary, the subgrains separate. Subsequently, coalescence of the subgrains may take place. In the latter situation, the subgrain boundary shows aluminium enrichment. With longer stirring time, coalescence and clustering of the smaller particles are

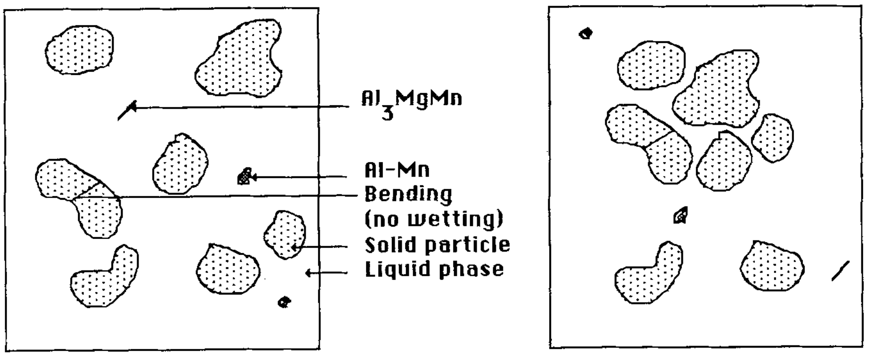

(a) Breaking of the dendrites during stirring

(b) During the isothermal hold

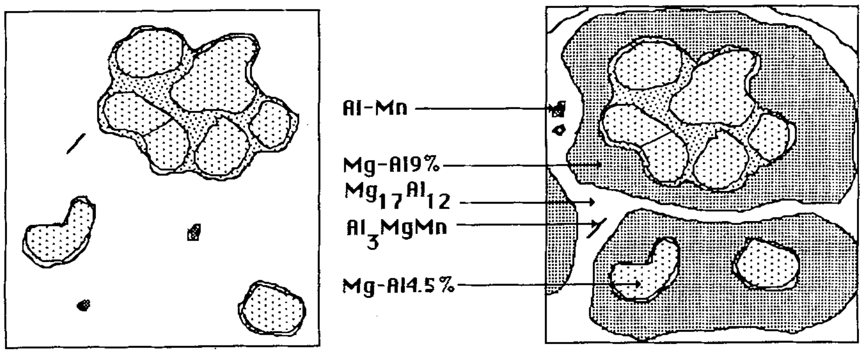

(c) At the end of stirring

(d) Upon complete solidification

Figure 13 Schematic diagram depicting the evolution of the rheocast microstructure.

more effective, and one observes more rounded particles (Fig. 13b). In addition, during stirring, homogenization of magnesium occurs within the primary rosette shaped cells.

Once stirring of the slurry ceases, the primary cells form a "bridge" structure, very similar to the three-dimensional network chain formation in polymeric materials, which explains why the viscosity of the slurry drastically increases when stirring stops.

The cooling rate experienced between T^* and the eutectic temperature T_e seems to be an important factor, because during this temperature excursion, the last liquid in the structure solidifies. Below T_e, the sample is solidified and the morphological changes and phase transitions occur in the solid state. At T_e, the remaining liquid freezes and decomposes into massive $Mg_{17}Al_{12}$ compound and into a magnesium-rich lamellar phase whose appearance blends into that of the adjacent primary solid solution. As expected, the large AlMn precipitates are enveloped by the $Mg_{17}Al_{12}$ phase as shown in Fig. 13d.

The major difficulty and limitation of rheocast samples is that one cannot directly examine the structural features of the slurry on an on-line basis; for example, the structure at the beginning of agitation, and the structure when agitation ceases immediately before the impeller is removed. One has to rely on indirect analysis methods, specifically

(i) etching techniques (see Fig. 10),

(ii) reheating experiments to delineate the primary phase from the surrounding matrix (see Fig. 11), and

(iii) scanning microscopy of the rheocast samples to delineate the cells via backscattering techniques.

Agreement of these three different techniques confirms our interpretation of the evolution of the rheocast structure.

It is clear from these results that rheocasting of AZ91D alloy gives rise to a "composite-like" structure having many advantages. Based on this study of processing – structure relationships, the effect of each processing variable on the resultant structure has been demonstrated. However, there are counteracting effects and depending on the desired end-result, a judicious choice for the optimum conditions must be made. For example, a high isothermal hold temperature (corresponding to a low fraction solid present) gives rise to a bimodal distribution of cells whereas a low isothermal hold temperature tends to give rise to a unisize distribution. On the other hand, a long stirring time (at the hold temperature) decreases this polarization of size distributions. Thus, one needs to select a set of processing conditions depending on the desired end-result.

One of the major disadvantages of such a laboratory batch-type processing study is the inevitable presence of large amounts of porosity. Unfortunately, the rheocast samples suffered from this as evidenced by the mechanical property results. The subsequent thermomechanical processing rectified the porosity problem, and the mechanical properties of the extruded samples are quite outstanding. Furthermore, if rheocasting is carried out in a continuous fashion (in a production-type set-up), the porosity problem will be alleviated. Overall, the observations from this study are in relatively good agreement with the results published by researchers who have investigated the rheocasting of other non-ferrous or ferrous systems.

7. Conclusions

1. Magnesium-based alloys, and specifically alloy AZ91D, can be rheocast. The rheocast structure of alloy AZ91D is unique and different when compared to the structure in die-cast or sand-cast components. In the rheocast material a dendritic network is not observed. The dendritic islands are broken up during agitation, resulting in the formation of spherical or rosette-like cells. The rheocast structures consist of coarsened and rosette-like primary cells surrounded by divorced eutectic phases. The results indicate that the average size of the primary island is 200 μm.

2. The composition of the rosette-like cell is 94.9 wt % Mg, 4.5 wt % Al, 0.5 wt % Zn, 0.1 wt % Mn. The envelope surrounding the cells is the last liquid to freeze and is rich in solute aluminium; it solidifies as a divorced eutectic.

3. There are three key processing variables affecting the resultant rheocast structure: the rheocasting temperature, the stirring time and the imposed shear rate. As the rheocasting temperature decreased (increasing volume fraction solid present), a noticeable uniformity of the primary cell size and an increase in their sphericity was observed. Long stirring times had the same effect. Increasing the shear rate, on the other hand, gave rise to a more efficient break-up of the dendritic structure. Though the cooling rate of the rheocast slurry as it related to the final resultant structure was not a major parameter in this study, it is believed that the solidification rate following removal of the impeller is an important and significant parameter. It is recommended that future work should take this into account.

4. The extruded as-cast and rheocast AZ91D samples have a higher strength and higher ductility than the as-cast material. Such a combination of strength and ductility is very desirable, and points out the potential of this material as a wrought alloy.

Acknowledgements

The authors are grateful to Pechiney Corporation for sponsoring the VSNA (Volontaire du Service National Actif) programme at Drexel University, under which one of us (A.T.) is a Visiting Scientist, and especially to Dr Jean Bouvaist who is at the origin of this work. The authors also want to thank Professor Roger Doherty for the many helpful discussions and his insight, and to acknowledge the technical assistance of the Voreppe team of Mr Philippe Bridot, Mr Vincent Chastagnier and Dr Véronique Laurent.

References

1. F. C. BENNETT, R. E. LEONTIS and S. L. COULING, in Proceedings of 34th Meeting of the International Magnesium Association, 1977, p. 23.
2. S. C. ERICKSON, in Proceedings of 44th Annual World Magnesium Conference, Tokyo, 1987, p. 39.
3. M. C. FLEMINGS, In Proceedings of Workshop held at

the Army Materials and Mechanics Research Center, Massachusetts; MCIC Report MCIC 78-35 (1978) p. 3.

4. R. A. JOLY and R. MEHRABIAN, *J. Mater. Sci.* **11** (1976) 1393.
5. A. VOGEL, DPhil thesis, University of Sussex (1977).
6. R. MEHRABIAN and M. C. FLEMINGS, *Trans. AFS* **80** (1972) 175.
7. H. I. LEE, DPhil thesis, University of Sussex (1982).
8. E. F. FASCETTA, R. RICK, R. MEHRABIAN and M. C. FLEMINGS, *Trans. AFS* **81** (1973) 95.
9. D. B. SPENCER, R. MEHRABIAN and M. C. FLEMINGS, *Metall. Trans.* **3** (1972) 192.
10. R. G. RICK, A. VRACHNOS, K. P. YOUNG, N. MATSUMOTO and R. MEHRABIAN, *Trans. AFS* **83** (1975) 25.
11. Y. V. MURTY, D. G. BACKMAN and R. MEHRABIAN, in Proceedings of Workshop held at the Army Materials and Mechanics Research Center, Massachussetts; MCIC Report MCIC 78-35 (1978) p. 95.
12. V. LAXMANAN, MS thesis, Massachusetts Institute of Technology (1975).
13. M. C. FLEMINGS, R. G. RICK and K. P. YOUNG, *Mater. Sci Engng* **25** (1976) 103.
14. R. MEHRABIAN, R. G. RICK and M. C. FLEMINGS, *Metall. Trans.* **5** (1974) 1899.
15. S. D. E. RAMATI, G. J. ABBASCHIAN and R. MEHRABIAN, in Proceedings of Workshop held at the Army Materials and Mechanics Research Center, Massachusetts; MCIC Report MCIC 78-35 (1978) p. 85.
16. S. D. E. RAMATI, D. G. BACKMAN, Y. V. MURTY, G. J. ABBASCHIAN and R. MEHRABIAN, *ibid.* p. 13.
17. R. D. DOHERTY, M. I. LEE and E. A. FEEST, *Mater. Sci. Engng* **65** (1984) 181.
18. A. VOGEL and B. CANTOR, *J. Crystal Growth* **37** (1977) 309.
19. J. J. A. CHENG, D. APELIAN and R. DOHERTY, *Met. Trans. A.* **17A** (1986) 2049.
20. D. APELIAN, in "Advanced Casting Technology", AGARD Conference Proceeding No. 325, Brussels (NATO, Neuilly sur Seine, France, 1982) p. 6.
21. A. VOGEL, R. D. DOHERTY and B. CANTOR, in Proceedings of International Conference on Solidification, University of Sheffield, Sheffield, England (Metals Society, London, 1977) p. 518.
22. Metals Handbook, 9th Edition, 1986, Vol. 2 (American Society for Metals, Metals Park, Ohio) p. 427.

Received 4 January
and accepted 3 May 1989